# A Recognition Algorithm of VGPO Jamming Based on Discrete Chirp-Fourier Transform

**Chuanzhang Wu**
Xidian University
**Baixiao Chen** ( bxchen@xidian.edu.cn )
Xidian University https://orcid.org/0000-0001-7320-327X

**Research**

**Keywords:** Deceptive jamming, Discrete chirp-Fourier transform, Jamming recognition, Feature extraction

**Posted Date:** June 24th, 2020

**DOI:** https://doi.org/10.21203/rs.3.rs-21374/v2



**Version of Record:** A version of this preprint was published on August 17th, 2020. See the published version at https://doi.org/10.1186/s13634-020-00694-3.

RESEARCH

# A Recognition Algorithm of VGPO Jamming Based on Discrete Chirp-Fourier Transform

Chuanzhang Wu and Baixiao Chen*

**Abstract**

This paper addresses the recognition problem of velocity gate pull-off (VGPO) jamming from the target echo signal for the velocity-based tracking system. The discrete chirp-Fourier transform (DCFT) is studied in this paper to jointly estimate the chirp rates and frequencies of the target and jamming signals. Firstly, the scaling characteristic of the DCFT algorithm is explored. Then we focus on the quantitative effect of the VGPO jamming signal by analyzing the jointly estimated results in each pulse. The quantitative effect indicates that, as long as the estimated frequency is unchanged, the relationship between the estimated chirp rate and the pulse numbers is similar to the relationship between the frequency offset of VGPO jamming and the time. Finally, by utilizing the joint estimated results in each pulse repetition interval and calculating the mean square to variance ratio (MSVR) of the normalized estimated chirp rate, the VGPO jamming can be recognized. Simulation results show that the jamming signal and the target echo become distinguishable with the proposed feature. Comparing to the existing works, the proposed method can correctly recognize the jamming signal with lower jamming-to-noise ratio (JNR) 5dB with less data needed, which means it can work effectively in the early stage of interference implementation and shows great potential in practical applications.

**Keywords:** Deceptive jamming; Discrete chirp-Fourier transform; Jamming recognition; Feature extraction

## 1 Introduction

Electronic countermeasure (ECM) has always been an important research direction in radar [1, 2]. As a typical category, the deceptive jamming is often used to deceive a hostile radar system by generating a large number of active false targets in terms of direction, position, and velocity [3]. With the widespread application of the digital radio frequency memory (DRFM) technique, the interference effect of ECM is further reinforced. In a DRFM system, the intercepted radar signal is firstly down-shifted in frequency. And then it is sampled with an analog-to-digital converter and stored in a high-speed digital memory where the samples can be manipulated in amplitude, frequency, and phase to produce desired deceptive signals. When being recalled, the stored samples are processed by a digital-to-analog converter, and then transmitted back to the victim radar [4].

Over several decades, with the continuous development of ECM, the electronic counter-countermeasures (ECCM) are also studied by more and more researchers. Many methods for recognizing and countering deceptive jamming are studied based on the DRFM technique. In 2006, Maria analyzed the phase and delay quantization effect of the DRFM device in detail [5]. In [6], she further defined the difference between the deceptive jamming and the target echo in the frequency domain as the jamming signal error angle which is introduced by the DRFM system and proposed a detection method.

Furthermore, many researchers counter the jamming signal from the aspect of jamming detection. In [7], the authors presented the adaptive detection schemes and the enhanced adaptive sidelobe blanking algorithms, which consider the scenario in realistic when a mismatched signal is present in the data. In [8], they proposed an new algorithm to detect the coherent signals from noise, clutter and noise-like interference. For the same problem, two dataset are utilized at the design stage to get receiver adaption, and a two-stage detector is recommended [9]. In [10], the authors conceived a multiple-stage adaptive architectures to detect the target, and shows a better performance compared to the two-stage detector in [9].

What's more, the jamming signal can also be distinguished from the target according to their difference

*Correspondence: bxchen@xidian.edu.cn
National Laboratory of Radar Signal Processing, Xidian University, Taibai South Road, 710071, Xi'an, China
Full list of author information is available at the end of the article

in various domains. In [11], the authors found the difference between the deceptive jamming and the target echo by calculating their product spectrum matrix. In [12], the deceptive jamming is analyzed in the spatial frequency domain in the multiple-input multiple-output system with frequency diverse array and suppressed in the joint transmit-receive domain. Moreover, the deceptive jamming and its anti-jamming methods in some new radar systems are also studied [13, 14].

Although the range gate-pull off (RGPO) in DRFM devices has been studied by many researchers [15, 5], not many published literature on the velocity gate pull-off (VGPO) jamming about the recognition and countering problem are available. In [16], the authors proposed an approach to suppress the velocity deception jamming by designing adaptive initial phases in the pulse repetition interval (PRI) domain. This method is further applied in the cognitive radar system [17]. In [18], a VGPO jamming countermeasure is proposed by utilizing the front-back-edge tracking gate, while it has to judge the jamming pulling off direction first. These methods are based on waveform design and radar systems respectively. By drawing on the texture feature in image recognition, Yang converted the time-frequency image of the jamming signal into a gray image, and then extracted the image feature based on the Zernike moments and recognize the jamming signal [19]. Although this method can recognize various jamming signals in a single pulse, it requires that there are some distinct differences in the time-frequency domain among various kinds of jamming signals. In other words, it can only be effective after the pull-off jamming has been implemented for a long time.

The purpose of this paper is to approach a recognition algorithm towards the VGPO jamming. To this end, the joint estimation algorithm of the chirp rate and frequency is introduced. Different from the method in [19], we analyze the theoretical estimation results of chirp rate and frequency in each pulse, and then extract the feature about the estimated chirp rate to distinguish the VGPO jamming and target.

Currently, many methods are available on joint estimation, such as maximum-likelihood [20], adaptive chirplet transform [21] and phase function [22]. However, the theoretical value of the rate of frequency of the jamming signal is far less than the minimum interval in the chirp rate domain in a general way. Consequently, most of these methods will lose efficacy. For the discrete chirp-Fourier transform (DCFT) algorithm[23], it is generalized from the discrete Fourier transform (DFT). Besides matching the multiple frequency similar to the DFT algorithm, it uses the multiple chirp components to match the chirp rates. Most important of all, it can increase the resolution in the chirp rate domain by introducing a scaling factor, which is termed as the scaling property and will be analyzed in this paper. As a result, it is still applicable in this situation. Nowadays, it has applied in many cases [24, 25].

This paper is organized as follows. In Section 2, the received signal models of both real target echo and VGPO jamming are first formulated, then we introduce the modified DCFT and analyze its scaling property, and derive the estimated chirp rate and frequency in each pulse repetition interval (PRI), and further define a new feature parameter. Section 3 shows the simulation results. Section 4 is the concluding remarks.

## 2 Methods

In this section, we elaborate on the theory and the method of jamming signal recognition. First, we present the signal models for VGPO jamming and target echo. Second, we introduce the modified DCFT and study its scaling property. Then, the quantitative effect is analyzed when performing the joint estimation with the DCFT algorithm, and it is also discussed in the non-linear scenario. Finally, we define a feature to distinguish the VGPO jamming and the target echo.

### 2.1 Signal Model

The whole process that a jammer implements VGPO interference can be divided into three steps: pull-off halting, pulling off, and closing [3]. After the radar signal is intercepted, the jammer retransmits the signal with a Doppler frequency shift inflicted on. To deceive the radar effectively, the power of the jamming signal is always greater than that of the real target echo. Therefore, the tracking loop of the radar would track the false Doppler frequency, and be slowly pulled away from the velocity gate of the real target.

Assume the signal transmitted by radar is $s(t)$. Then the signal reflected by a hypothetical target in the far-field can be modeled as [16]

$$s_r(t) = A_r s(t - t_r) e^{j2\pi f_d (t - t_r)} + n(t) \tag{1}$$

where $A_r$ and $t_r$ denote the reflection coefficient and the time delay of the hypothetical target respectively, and $f_d$ is its Doppler frequency.

Comparing with the real target echo, the VGPO jamming has a pseudo-Doppler frequency shift based on $f_d$. For convenience, we consider the scenario that only one interference exits, and the jamming signal can be expressed as

$$s_J(t) = A_J s(t - t_J) e^{j2\pi f_{dj} (t - t_J)} + n(t) \tag{2}$$

where $A_J$ denotes the equivalent reflection coefficient of the interfering source, $t_J = t_r + \Delta t_d$ is the jamming

propagation delay, and $\Delta t_d$ is the time delay of jammer relay which is often far less than $t_r$, $f_{dj} = f_d + \Delta f_d$ is the modulated pseudo-Doppler frequency. Here, we define jamming-to-noise ratio (JNR) $A_J^2/\sigma^2$, and signal-to-noise ratio (SNR) $A_r^2/\sigma^2$, where $\sigma^2$ is the variance of Gaussian noise $n(t)$, and jamming-to-signal ratio (JSR) is defined as JNR-SNR.

Similar to the RGPO system described in [5, 26], a VGPO system should linearly increase the frequency offset to create a series of constant velocity-rate false targets. This scenario is also the one we often use when analyzing VGPO [19, 27, 28], and is equivalent to the constant acceleration profile in the range domain. Then the $f_{dj}$ at the $m$th PRI can be expressed as [28]:

$$f_{dj} = V_f[t + (m-1)T_r] + f_d \tag{3}$$

where $V_f$ denotes the slope of $f_d$ with respect to $t$ which is also called acceleration, $T_r$ denotes the pulse repetition period.

To enable radar accurately capture and track the velocity loop of the jamming signal, $V_f$ won't be greater than the maximum trackable acceleration of a target to radar [1]. On the other side, $V_f$ won't be particularly small for implementing interference effectively and protecting the real target. In a word, $V_f$ has a reasonable value range.

Substitute (3) into (2), and we can find that, despite the signal form, the VGPO jamming signal is a chirp function with a chirp rate of $V_f$. This is the inspiration for the jamming identification in this paper.

As the specific form of $s(t)$ is not assumed, we may have to do some preprocessing to prevent the influence of the potential time-varying frequency components in signal form on chirp rate estimation. The preprocessing may be different for various kinds of signals. Take the widely used linear frequency modulation (LFM) signal as an example, it has a quadratic term in terms of $t$, i.e., the inherent chirp rate. Generally speaking, the acceleration $V_f$ of the VGPO jamming (three times the acceleration of gravity in X-band is about 2kHz/s) is much smaller than the chirp rate of LFM signal (typical value $10^{10} - 10^{14}$ Hz/s, [1]). As a result, the dechirping processing should be performed first in the recognition procedure for the radar that emits LFM signal.

After being sampled with discrete-time $t = nT_s$ where $T_s$ denotes the sampling interval, and performing some appropriate preprocessing, the jamming signal $s'_J(t)$ in $m$th PRI can be expressed as

$$\begin{aligned} s_J(n) &= s'_J(t)\Big|_{t=nT_s} \\ &= A_J \exp\{j2\pi(V_f n^2 T_s^2 + f'_{dj} n T_s) + j\varphi_j\}, \end{aligned} \tag{4}$$

where

$$f'_{dj} = f_d + (m-1)V_f T_r - V_f t_J + f_{d0}, \tag{5}$$

$$\varphi_j = -2\pi(f_d + (m-1)V_f T_r)t_J + \varphi_0, \tag{6}$$

where $f_{d0}$ and $\varphi_0$ separately denote the time-invariant frequency and constant phase term in $s_J(n)$.

The phase of the discretized jamming signal in (4) contains three components, a quadratic item with respect to $nT_s$ with a coefficient $V_f$, a linear item with respect to $nT_s$ with a coefficient $f'_{dj}$ and a time-independent item $\varphi_j$. Ignoring the time-independent phase item, the coefficient $f'_{dj}$ of the linear item is different in various PRIs, while the coefficient of the quadratic phase items are the same. However, the following analysis indicates that the quantization in the frequency domain will influence the estimated result in the chirp rate domain when performing joint estimation to the jamming signal.

### 2.2 Discrete Chirp-Fourier Transform and its Scaling Property

The discrete chirp-Fourier transform algorithm is used to jointly estimate the chirp rate and the frequency of a chirp-type signal. For an analog chirp signal $x(t) = \exp[j2\pi(k_0 t + l_0 t^2)]$ $(0 \le k_0, l_0 \le N-1)$, its discretized form with sample rate $1/N$ is

$$x_I(n) = W_N^{-(k_0 n + l_0 n^2/N)} \tag{7}$$

where $W_N = \exp(-j2\pi/N)$. The corresponding $N$-point DCFT of signal $x_I(n)$ is defined as [29]

$$X_c(k,l) = \frac{1}{\sqrt{N}} \sum_{n=0}^{N-1} x_I(n) W_N^{kn + ln^2/N}, 0 \le k, l \le N-1 \tag{8}$$

where $k$ and $l$ represent the frequency and chirp rate variable respectively.

In (7), the duration of the signal is normalized as 1, which makes both of $k$ and $l$ are less equal than the length of signal $N$. In radar signal processing, the Doppler frequency of the signal is less than the sampling frequency of $f_s$, and the chirp rate is less than $f_s^2$ correspondingly. After sampling with discrete-time $t = nT_s$, the discretized form of $x(t)$ is rewritten as

$$x(n) = \exp[j2\pi(k_0 n T_s + l_0 n^2 T_s^2)] \tag{9}$$

where $0 \le k_0 < f_s, 0 \le l_0 < f_s^2$. To maintain the consistency between the estimated values of frequency

and chirp rate and the actual ones, the corresponding form of DCFT should be modified as

$$X_{mc}(k,l) = \frac{1}{\sqrt{N}} \sum_{n=0}^{N-1} x(n) W_N^{kn+ln^2}, 0 \le k,l \le N-1 \tag{10}$$

Each bin in frequency domain and chirp rate domain represents $f_s/N$ and $f_s^2/N$ respectively. When $|X_{mc}(k,l)|$ maximizes, the estimated values of $k$ and $l$ are

$$k = k_0 N T_s, l = l_0 N T_s^2 \tag{11}$$

respectively, and the corresponding estimated values of frequency and chirp rate are $k_0$ and $l_0$ respectively.

Essentially, the time delay of a signal is equivalent to zero-padding in front of the signal. It changes the phase of the signal's DFT result, while the estimated frequency and the envelope of DFT results are unchanged. In a very short timestamp, the positions of target and jammer are usually considered to be located in the same range cell. Under this assumption, both of the time delay $t_r$ and $t_J$ are constant, which means the number of zero paddings in each PRI is the same during this period. In other words, the time delay in these PRIs won't influence the estimated value of frequency through DFT. As the DCFT algorithm is a generalized form of the DFT algorithm, this conclusion is applicable for jointly estimating the values of chirp rate and frequency with the DCFT algorithm.

From (10), one can see that the chirp rate variable only appears in the factor $W_N^{ln^2}$. It means that the chirp rate domain of DCFT can be broadened or compressed after dividing the variable $l$ by a scaling factor $C$, which equivalently increases or decreases the minimum interval in the chirp rate axis. According to the scalability of the DCFT algorithm in the chirp rate domain, we further define the modified DCFT as follows

$$X'_{mc}(k,l) = \frac{1}{\sqrt{N}} \sum_{n=0}^{N-1} x(n) W_N^{kn+ln^2/C} \tag{12}$$

At this time, the maximum value in the chirp rate axis changes from $f_s^2$ to $f_s^2/C$, and the corresponding minimum interval decreases to $f_s^2/NC$. Similarly, for the chirp signal in (9), the peak position in the modified DCFT domain is located at

$$k = k_0 N T_s, l = l_0 N C T_s^2, \tag{13}$$

and the corresponding values of frequency and chirp rate are $k_0$ and $l_0$ respectively. It indicates that the estimated values of chirp rate and frequency are unchanged in the modified DCFT compared with the DCFT in (10).

As mentioned above, the value of $V_f$ is in a reasonable range. What's more, the sampling frequency $f_s$ is always known as prior information. As a result, the scaling factor $C$ has a rough estimation for the radar side. The bigger the scaling factor $C$, the smaller the minimum interval in the chirp rate domain for the modified DCFT algorithm. In fact, if $C$ is big enough or much bigger than $N$, the DCFT result for different $l$ is almost the same. In this case, the DCFT algorithm is considered as degenerating into the DFT algorithm and could cause a huge estimation error to the chirp rate at low SNR.

### 2.3 The Analysis of Quantitative Effect

In this part, we analyze the influence of a small frequency offset on the DCFT estimation results. In the DFT algorithm, we estimate the constant frequency $f_{n0}$ of a signal by matching it with a quantitative value in frequency domain, i.e., $f_{n0} = n_0 f_s/N$, where $N$ is the total number of DFT, $n_0 (0 \le n_0 < N-1)$ is a certain nonnegative integer. When the signal's frequency $f_{n1}$ has an offset $\Delta f$ based on $f_{n0}$, i.e.,

$$f_{n1} = f_{n0} + \Delta f, \tag{14}$$

the peak still exhibits at the position $f = f_{n0}$ only if $|\Delta f| < f_s/2N$. It means the frequency offset $\Delta f$ is ignored due to the quantization in the frequency domain.

Similarly, the quantization error must occur in the DCFT algorithm as well. From [23], it is pointed out that, for a discrete chirp signal

$$\tilde{x}(n) = W_N^{-(\tilde{k}_0 n + \tilde{l}_0 n^2)}, \tag{15}$$

its DCFT result has the similar peak property as the signal $x(n) = W_N^{-(k_0 n + l_0 n^2)}$, where $\tilde{k}_0$ and $\tilde{l}_0$ close to integers $l_0$ and $k_0$ respectively, i.e.

$$|\tilde{l}_0 - l_0| < \epsilon \quad and \quad |\tilde{k}_0 - k_0| < \eta \tag{16}$$

where $\epsilon$ and $\eta$ are two arbitrary positive values. However, this conclusion is drawn based on the condition that $\tilde{l}_0$ and $\tilde{k}_0$ are close enough to $l_0$ and $k_0$, i.e., $\epsilon, \eta \approx 0$. As the process of pulling off a velocity gate is continuous, the pseudo Doppler frequency of the jamming signal changes in each PRI. Moreover, the minimum interval in the chirp rate axis decreases after adopting the modified DCFT in (12). As a result, it becomes very necessary to analyze the quantitative effect of the DCFT algorithm in this paper.

For a discrete VGPO jamming in (4), its modified DCFT after ignoring the time-independent phase item $\varphi_j$ can be calculated by

$$\begin{aligned} X'_{mc}(k,l) &= \frac{1}{\sqrt{N}} \sum_{n=0}^{N-1} s_J(n) W_N^{kn+ln^2/C} \\ &= \frac{A_J}{\sqrt{N}} \sum_{n=0}^{N-1} e^{j2\pi(V_f n^2 T_s^2 + f'_{dj} n T_s - kn/N - ln^2/NC)} \end{aligned} \tag{17}$$

Let the Doppler frequency

$$f'_{dj} = \tilde{f}_{dj} + \Delta f_m \tag{18}$$

where $\tilde{f}_{dj}$ is an integer multiple of $f_s/NC$, and $\Delta f_m$ denotes the remainder Doppler frequency besides $\tilde{f}_{dj}$ in $m$th PRI. Here, we assume the total number of pulses is $M$ when the estimated frequency through the modified DCFT is fixed as $\tilde{f}_{dj}$. Then we have $0 \le m \le M-1$ and $0 \le \Delta f_m < \Delta f_M < f_s/NC$.

For the convenience of representation, we let $\tilde{f}_{dj} = f_d - V_f(T_r + t_J) + f_{d0}$, and $\Delta f_m = mV_f T_r$ according to (5) and (18). Then (17) can be rewritten as follows

$$X'_{mc}(k,l) = \frac{A_J}{\sqrt{N}} \sum_{n=0}^{N-1} e^{j2\pi\phi_1} e^{j2\pi\phi_2}, \tag{19}$$

where $\phi_1(n) = (V_f T_s^2 - \frac{l}{NC})n^2 + mnV_f T_r T_s$ and $\phi_2(n) = (\tilde{f}_{dj} T_s - k/N)n$.

Let

$$P = \left| \sum_{n=0}^{N-1} e^{j2\pi\phi_1} e^{j2\pi\phi_2} \right|. \tag{20}$$

In the complex coordinates system, each complex exponential can be regarded as a unit vector. Consequently, $P$ can be considered as the modulus of a vector summed by $N$ unit vectors, and it reaches to maximum of $N$ when all of the vectors point in the same direction. According to [23], $P$ maximizes when the frequency variation of DCFT matches to the quantized frequency $\tilde{f}_{dj}$, i.e. $\phi_2 = 0$. Then we have

$$k = N\tilde{f}_{dj}/f_s \tag{21}$$

On the other side, $\phi_1(n)$ differs by an integer to various $n$,

$$\phi_1(n_1) = \phi_1(n_2) + \varphi_{0n} \tag{22}$$

where $n_1$ and $n_2$ are two arbitrary different integers between 0 and $N-1$, $\varphi_{0n}$ is an integer. Substituting the expression of $\phi_1$ into (22), we can yield

$$(V_f T_s^2 - \frac{l}{NC})(n_1 + n_2) + mV_f T_r T_s = \frac{\varphi_{0n}}{n_1 - n_2} \tag{23}$$

Let $\alpha_1 = \varphi_{0n}/(n_1 - n_2)$, and $\alpha_2 = n_1 + n_2$. Then, if $P$ reaches to maximum $N$, it implies that the variable $l$ to arbitrary $n_1$ and $n_2$ in (23) is solvable, i.e.,

$$l = NC(V_f T_s^2 + \frac{mV_f T_r T_s - \alpha_1}{\alpha_2}) \tag{24}$$

The effective value of $\phi_1$ only exists in the fractional part from 0 to 1 due to the periodicity of the exponential function. Correspondingly, the true value of $l$ is the remainder after dividing by $N$ in (24). In other words, for a fixed $m$, the true value of $l$ should be fixed, too.

From (24), one can see that $l$ and $m$ are linearly related. In general, not all vectors in (20) point in the same direction, and $P$ can not reach to maximum $N$. $\varphi_{0n}$ in (22) is not an integer anymore to a fixed pair of integers $n_1$ and $n_2$, which changes the estimated chirp rate of jamming signal in $m$th PRI. Among various PRIs, $m$ is the unique determining factor that influences the value $P$, and the estimated chirp rate $l$. From this point, $\varphi_{0n}$ is not an integer either for various pairs of $n_1$ and $n_2$. However, it can be found from the formulation of $\phi_1$ that, $\varphi_{0n}$ is linearly related to $m$ for fixed $n_1$ and $n_2$. It means $l$ is still proportional to $m$. As

$$mnV_f T_r T_s = nT_s \Delta f_m < \frac{n}{NC} \le \frac{n^2}{NC}, \tag{25}$$

the influence of $m$ to $\phi_1(n)$ and $l$ is small. Once $V_f$ is fixed, all integer pairs $n_1$ and $n_2$ that makes $P$ reach to the maximum value (not $N$) are basically determined. Therefore, the slope between $l$ and $m$ can be considered to be unchanged at this time.

More generally, $\Delta f$ includes an extra frequency independent of $m$ (part of $\tilde{f}_{dj}$) which results in $\varphi_{0n}$ is not an integer either. Then the estimated chirp rate of VGPO jamming in $m$th PRI may differ form the one in (24), while the linear relationship between $l$ and $m$ still exists.

It can be seen that, when a joint estimation of the VGPO jamming with the DCFT algorithm is performed, the quantization in frequency domain will affect the estimated value of the chirp rate, and the estimated chirp rate is linearly related to the residue of the quantized frequency item.

Unlike in (3), we next discuss a more general scenario that the false target is maneuvering, which means $f_{dj}$ has a non-linear correlation with time $t$. Taking the quadratic relation as an example, $f_{dj}$ changes as follows over time $t$:

$$f_{dqj} = A_f[t+(m-1)T_r]^2 + V_f[t+(m-1)T_r] + f_d, \quad (26)$$

where $A_f$ is the cubic coefficient of time $t$.

Substituting the $f_{dj}$ in (2) with $f_{dqj}$, and following the same derivation from (4)∼6 and (17)∼(19), we can calculate the modified DCFT of the jamming signal in non-linear scenario. Similar to (5), the frequency item of the preprocessed jamming signal $f'_{dqj}$ can be expressed as follows

$$\begin{aligned} f'_{dqj} = {} & A_f n^2 T_s^2 + [V_f + 2A_f(m-1)Tr - A_f t_J] n T_s \\ & + \Delta f'_m + f_d - V_f t_J \end{aligned} \quad (27)$$

where

$$\Delta f'_m = A_f(m-1)^2 T_r^2 + (V_f - 2A_f t_J)(m-1)T_r \quad (28)$$

Still, we let $\phi'_1(n)$ be the function that includes high order terms of $n$ and $\Delta f'_m$, i.e.,

$$\begin{aligned} \phi'_1(n) = {} & A_f n^3 T_s^3 + [V_f + 2(m-1)A_f T_r] n^2 T_s^2 \\ & + \Delta f'_m n T_s - l n^2 / NC. \end{aligned} \quad (29)$$

Obviously, besides a cubic item of $nT_s$, there is a quadratic item of $n$ with respect to $m$, and a linear item of $n$ with respect to $m^2$ in $\phi'_1(n)$. With the same condition as in (22), we can find that there is a quadratic relation between $l$ and $m$ in this situation. More generally, the relationship between $l$ and $m$ is same with that between $f_{dj}$ and $t$. Here, we term this phenomenon as a quantitative effect.

Therefore, it can be concluded that, a series of small offsets in frequency would increase the values of the chirp rate in joint estimation. The quantitative effect can be interpreted as, within the timestamp when the estimated quantized frequency is unchanged, the estimated chirp rate of the VGPO jamming through the modified DCFT algorithm increases with a tendency that is the same as the relationship between $f_{dj}$ and $t$.

### 2.4 Feature Extraction

In this part, we use an identification parameter to benchmark the quantitative effect. As the pull-off stage of VGPO jamming continues for several seconds [1], the quantitative effect will appear periodically. For the real target echo, the estimated chirp rate through the modified DCFT algorithm is essentially the estimation error caused by thermal noise. Its value equals 0 in an ideal case, and randomly changes under noisy environment. By utilizing the distinctive quantitative effect, the VGPO jamming can be distinguished from the real target echo.

Here, we define the feature, the mean square to variance ratio (MSVR) of the normalized estimated chirp rate, and utilize it to distinguish the VGPO jamming and the real target echo. Let $C_e(m)$ represent the estimated chirp rate in $m$th PRI, and its normalized form is yield by

$$C'_e(m) = \frac{C_e(m) - C_e^{\min}}{C_e^{\max} - C_e^{\min}} \quad (30)$$

where $C_e^{\max}$ and $C_e^{\min}$ represent the maximum and minimum of $C_e$, respectively.

Let $\mathbf{C}'_e = [C'_e(1)\ C'_e(2) \cdots C'_e(m)]$, and the MSVR is defined as

$$\text{MSVR} = \frac{\mu_c^2}{\sigma_c^2} \quad (31)$$

where $\mu_c$ and $\sigma_c$ stand for the mean and the variance of $\mathbf{C}'_e$ respectively.

From the aforementioned content, it is concluded that $C_e(m)$ of VGPO jamming linearly (or nonlinearly) increases in $M$ PRIs. Although the estimated chirp rate is normalized from 0 to 1, its variance becomes smaller and smaller as the JNR increases. On the contrary, all of the elements in $\mathbf{C}_e$ of real target echo can be regarded as random, which means its MSVR is steady. Consequently, the VGPO jamming signal and the real target echo can be recognized by setting a proper threshold.

The flowchart of the identification procedure to VGPO jamming based on the DCFT algorithm is provided in Fig. 1. After being sampled, the received signal is preprocessed. Then the chirp rate of the signal is estimated by the modified DCFT in each pulse. Finally, by calculating the value of MSVR with the estimated results in $M$ PRIs, the VGPO jamming can be identified from the target signal.

## 3 Results and Discussion

In this section, we conduct some simulation experiments to illustrate the performance of the proposed method in this article. We assume the waveform of the transmitted signal is LFM. It is worth noting that the pulse numbers is set relatively large in some simulations which is similar with [18]. This is because our method is performed from the time when the interference begins to implement, and the shifted frequency is small at the early pull-off stage and even within a single frequency interval.

### 3.1 Scaling Property

Firstly, we demonstrate the effectiveness of the scaling property of the modified DCFT algorithm. With the acceleration $V_f$ 50kHz/s for instance, we consider the scenario that $f_{dj}$ linearly changes with $t$ as shown in (3).

The carrier frequency is 10GHz. The bandwidth and time width of the signal is 5MHz and 100us respectively, and the pulse repetition period is 500us. The velocity of the target is fixed as 200m/s. The SNR and JNR are 5dB and 10dB respectively and the sampling frequency is 10MHz.

Both of the DCFT results of jamming signal and target echo and their corresponding profiles at the frequency where the $|X'_{mc}|^2$ maximizes, are shown in Fig. 2. In the first row, the scaling factor $C$ is 1 (without scaling). In the second and the third row, $C$ is $4e3$ and $2e7$ respectively. In the profiles, both of the modules of the DCFT results of jamming and target are normalized to 1 to compare the estimated chirp rate more visually, and the peaks of DCFT results of jamming and target are respectively signed by a red circle and a blue star.

By comparing the results shown in various rows in Fig. 2, it's easy to find that the DCFT result magnifies in the chirp rate domain as the scaling factor $C$ increases. The estimated chirp rates of target and jamming are distinguishable in Fig. 2(i), but not in Fig. 2(c) and Fig. 2(f). Although the estimated chirp rate is quite different from the parameter we set, it is not surprising to us, due to the existence of noise and the quantitative effect.

### 3.2 Quantitative Effect

In the second simulation, 500 pulses of jamming signal and target echo are respectively considered to verify the effectiveness of the quantitative effect. The radar signal's parameter is the same as above. Both of the linear and non-linear (quadratic) scenarios in (3) and (26) are considered. The $V_f$ is 20kHz/s, which is equivalent with the acceleration 200 m/s$^2$ in [28]. The $A_f$ is set to 100kHz/s$^2$ which is relatively large to obtain an intuitional result. The scaling factor of $C$ is 2e5. The JNR and SNR are 15dB and 10dB respectively. The estimated values of frequency and chirp rate of the target and linear VGPO in various pulses are shown in Fig. 3(a), and the ones of the target and quadratic VGPO are shown in Fig. 3(b). For comparison, we also plot the real shifted Doppler frequency of the jamming signal in each pulse.

The estimated frequency of the jamming signal stepwise increases in both linear and quadratic scenarios. In Fig. 3(a), the estimated chirp rate of the jamming signal increases linearly from 0s to 0.08s, and increases quadratically in Fig. 3(b), which is coincident with our theoretical analysis. It should be noticed that there always appears a flat area where the estimated chirp rate is 0 (e.g., from 0.062s to 0.074s in Fig. 3(b)). This is because the estimated frequency increases at this point, that is to say, $\tilde{f}_{dj}$ in (18) is quantized into the next frequency bin. Correspondingly, the remaining Doppler frequency $\Delta f_m$ has to subtract $f_s/N$, which causes the estimated chirp rate $l$ becomes negative. However, the value range of $l$ is form 0 to $N-1$. As a result, the estimated chirp rate $l$ becomes 0 which is the closest one to the theoretical value.

### 3.3 Influence of Difference Parameters to DCFT

We then explore the influence of different signal parameters, pulse numbers, and SNR (or JNR) on identifying the VGPO jamming by utilizing the proposed feature.

We assume the bandwidth of the signal is fixed as 5MHz, and the sampling frequency is 10MHz, while the pulse duration changes from 20us to 100us with duty cycle 20%. The carrier frequency is 15GHz, and the scaling factor $C$ is 2e5.

To inquire the question of how long it would take for the proposed method to identify the jamming signal successfully, we jointly consider the influence of the signal's time width and pulse numbers. The linear pull-off scenario is considered. $V_f$ is still set to 20kHz/s. The MSVR of the target echo and the VGPO jamming under various signal parameters and pulse numbers are shown in Fig. 4(a) and (b), respectively.

The MSVR of the target echo is steady around 0.45 after 100 pulses, even under different signal time width from Fig. 4(a). On the contrary, the MSVR of the VGPO jamming is various under different time width and different pulse numbers in Fig. 4(b), and its maximum is about 2.96. By comparing Fig. 4(a) and Fig. 4(b), we can find that the MSVR of jamming signal is always bigger than that of the target echo.

Overall, the MSVR of VGPO jamming increases as the number of pulses increases until the estimated frequency changes. The wider the time width, the faster the value of MSVR increases. It should be noticed that the ladder-shaped portion is caused due to a change in the estimated frequency.

We plot the profiles in Fig. 4(b) when time width are 50us, 80us and 100us respectively, and show them in Fig. 5. We also draw the lines corresponding to the number of pulses 100, 125, and 200. All intersections formed by the same color represent the same total time of interference implementation 0.05s, and the MSVR of these points are 2.89, 2.89, and 2.83 respectively. As a result, if we use the number of pulses with the same timestamp (the product of the pulse numbers and PRI)

to calculate the characteristic parameter, the MSVR under shorter time width scenario will be smaller as long as the estimated frequency does not change.

We then study the influence of SNR on the performance of the proposed feature. We consider the scenario when the pulse duration is 20us according to the result in Fig. 4(b), the total time of interference implementation is 0.08s (800 pulses).

Besides a target in uniform speed, an accelerated target with an acceleration 2.7 m/s$^2$, a linear and nonlinear pull-off VGPO jamming are also considered. The $V_f$ of the linear pull-off jamming is 2kHz/s. A nonlinear pull-off case is a simple form of the maneuvering scenario, and its $A_f$ is 20kHz/s$^2$. The JSR is fixed as 3dB, and the SNR changes from 0dB to 15dB. The relationships between MSVR and $SNR$ are shown in Fig. 6.

It can be seen that two kinds of VGPO jamming almost have the same MSVR. It means that the quadratic term of the frequency pull-off function in (26) has less effect on MSVR in a very short time (0.1s) if the coefficient of the quadratic term is not too large (e.g. 20kHz/s$^2$).

Different from the results of the linear and nonlinear VGPO jamming, the MSVRs of the target is almost steady which is similar to the result in Fig. 4(a). It means that the MSVR of the target signal is unchanged even with various parameters. Moreover, the MSVR of the target and the accelerated target are almost the same. Combined with the MSVR of the two jamming signals, we can conclude that a tiny acceleration or small maneuvering on target hardly changes the value of MSVR.

### 3.4 Discrimination Performance

Before we conduct the discrimination performance of the proposed method, we consider the influence of the speed of frequency offset, i.e., the value of $V_f$, on MSVR. The sampling frequency is 20MHz, and the SNR and JSR are 10dB and 5dB, respectively. The other parameters are the same as the previous subsection. The values of $V_f$ are separately assumed as 20kHz/s and 50kHz/s. The MSVR of target echo and jamming signal versus pulse numbers with various $V_f$ are shown in Fig. 7 where VGPO1 and VGPO2 separately denote the linear VGPO jamming with $V_f$ of 20kHz/s and 50kHz/s.

Apparently, the MSVR of the jamming signal with $V_f$ of 50kHz/s is larger than that of the jamming with $V_f$ of 20kHz/s. Furthermore, the more pulses involved in the calculation, the greater the MSVR of the jamming signal, which is consistent with the result in Fig. 4(b).

To compare the performance with the results in [18] and [19], 800 and 850 pulses are separately considered, with the same parameters in Fig. 6. The value of $V_f$ is set as 20kHz/s, 300 Monte Carlo trials are considered. As the value of MSVR of the target signal is sable under different radar parameters, the threshold can be set as the average between the minimum MSVR of the jamming signal, which is usually the corresponding value when the SNR is 0dB, and the stable value of MSVR of the target. In this simulation, the threshold is set as 0.65 as the MSVR of jamming signal is around 0.8 when the SNR is 0dB in Fig. 6. Fig. 8 shows the identification probability of jamming signal versus SNR based on the proposed method.

From Fig.8, when the SNR is 0dB, the identification probability of VGPO jamming could reach 0.975 with 850 pulses, and 0.81 with 800 pulses. When the SNR is 2dB, the jamming signal can always be correctly recognized.

From the aspect of the total data needed to correctly identify the jamming signal, our method only uses the signal data within 0.085s, and is less than the method in [18] which needs the signal data within 0.096s. From the aspect of the identification probability, our method can correctly recognize the jamming signal when the SNR is 2dB, which is smaller than that in [18] (the blue dotted line in Fig.8). It should be noted that the value of $V_f$ is 50kHz/s in [18], which also means our method would be better if the same value of $V_f$ is used based on the result in Fig. 7.

### 3.5 Discussion

Although this method can recognize the VGPO jamming with less data and a higher recognition rate compared to the open literature, it is not suitable for the jamming of range gate pull-off (RGPO) with uniform acceleration. This is because its chirp rate after dechirping is pretty small (about 0.2 for the false target with the same motion state with the same simulation parameters in this paper). However, as a more general form of VGPO, the range-velocity gate pull-off (R-VGPO) jamming can also be identified by this method. Even in mixed-signal including target echo and jamming, this method is still effective.

## 4 Conclusions

In this paper, the discrimination issue between the target echo and the VGPO jamming is studied. To this purpose, we resort the discrete chirp-Fourier transform to jointly estimate the chirp rate and frequency of a signal, and the scaling characteristic of the DCFT algorithm is studied and explored to increase the estimated accuracy in chirp rate domain. Based on the actual joint estimation results, the quantitative effect of the VGPO signal is further analyzed, it guarantees that the relationship between the pull-off acceleration

and the time can be judged from the relationship between the estimated chirp rate and the pulse numbers. To distinguish VGPO jamming and target echo, the MSVR is defined. Simulation results indicate that for a timestamp when the estimated frequency is unchanged, the MSVR of VGPO jamming increases with the pulse numbers and time width (with the same duty cycle) increases and is always larger than that of a target which is stable. Compared to other methods, the proposed can recognize the jamming signal with less data and have a higher recognition, it means a great potential in practical applications.

**Abbreviations**
VGPO: Velocity gate pull-off; DCFT: Discrete chirp-Fourier transform; MSVR: The mean square to variance ratio; JNR: Jamming-to-noise ratio; ECM: Electronic countermeasure; DRFM: Digital radio frequency memory; ECCM: Electronic counter-countermeasures; RGPO: Range gate pull-off; PRI: Pulse repetition interval; DFT: Discrete Fourier transform; SNR: Signal-to-noise ratio; JSR: Jamming-to-signal ratio; LFM: Linear frequency modulation.

**Ethic approval and consent to participate**
Not applicable.

**Consent for publication**
Not applicable.

**Availability of data and material**
Not applicable.

**Funding**
Not applicable.

**Competing interests**
The authors declare that they have no competing interests.

**Author's contributions**
Chuanzhang Wu found the idea and wrote this article, Baixiao Chen put forward some constructive suggestions for revision.

**Acknowledgments**
Thanks to the teachers and the students of the research group for valuable discussion and all the people who had put forward valuable suggestions.

**References**
1. Schleher, D.C.: Electronic Warfare in the Information Age, 1st edn. Artech House, Inc., USA (1999)
2. Poisel, R.A.: Information Warfare and Electronic Warfare Systems. Artech House, Inc., Norwood,MA (2013)
3. Jing, L.N., Ting, Z.Y.: A survey of radar ecm and eccm. IEEE Transactions on Aerospace and Electronic Systems **31**(3), 1110–1120 (1995). doi:10.1109/7.395232
4. Roome, S.J.: Digital radio frequency memory. Electronics Communications Engineering Journal **2**(4), 147–153 (1990). doi:10.1049/ecej:19900035
5. Greco, M., Gini, F., Farina, A., Ravenni, V.: Effect of phase and range gate pull-off delay quantisation on jammer signal. IEE Proceedings - Radar, Sonar and Navigation **153**(5), 454–459 (2006)
6. Greco, M., Gini, F., Farina, A.: Radar detection and classification of jamming signals belonging to a cone class. IEEE Transactions on Signal Processing **56**(5), 1984–1993 (2008)
7. Bandiera, F., Orlando, D., Ricci, G.: Advanced Radar Detection Schemes Under Mismatched Signal Models, (2009)
8. Bandiera, F., Farina, A., Orlando, D., Ricci, G.: Detection algorithms to discriminate between radar targets and ecm signals. IEEE Transactions on Signal Processing **58**(12), 5984–5993 (2010)
9. Carotenuto, V., De Maio, A., Orlando, D., Pallotta, L.: Adaptive radar detection using two sets of training data. IEEE Transactions on Signal Processing **66**(7), 1791–1801 (2018)
10. Yan, L., Addabbo, P., Hao, C., Orlando, D., Farina, A.: New eccm techniques against noiselike and/or coherent interferers. IEEE Transactions on Aerospace and Electronic Systems **56**(2), 1172–1188 (2020)
11. Xu, J., Liao, G., Zhu, S., So, H.C.: Deceptive jamming suppression with frequency diverse mimo radar. Signal Processing **113**(C), 9–17 (2015). doi:10.1016/j.sigpro.2015.01.014
12. Zhao, S., Zhang, L., Zhou, Y., Liu, N.: Signal fusion-based algorithms to discriminate between radar targets and deception jamming in distributed multiple-radar architectures. IEEE Sensors Journal **15**(11), 6697–6706 (2015). doi:10.1109/JSEN.2015.2440769
13. Zhao, S., Zhou, Y., Zhang, L., Guo, Y., Tang, S.: Discrimination between radar targets and deception jamming in distributed multiple-radar architectures. Iet Radar Sonar Navigation **11**(7), 1124–1131 (2017). doi:10.1049/iet-rsn.2016.0540
14. Sun, Q., Shu, T., Yu, K., Yu, W.: Efficient deceptive jamming method of static and moving targets against sar. IEEE Sensors Journal **18**(9), 3610–3618 (2018)
15. Li, W., Liu, W., Guo, L., Yang, X.: Joint slow/fast-time pulse diversity method for countering range gate pull off jamming. In: IET International Radar Conference 2015, pp. 1–4 (2015)
16. Zhang, J., Zhu, D., Zhang, G.: New antivelocity deception jamming technique using pulses with adaptive initial phases. Aerospace Electronic Systems IEEE Transactions on **49**(2), 1290–1300 (2013). doi:10.1109/TAES.2013.6494414
17. Xiong, W., Wang, X., Zhang, G.: Cognitive waveform design for anti-velocity deception jamming with adaptive initial phases. In: 2016 IEEE Radar Conference (RadarConf), pp. 1–5 (2016)
18. Wu, L., Fu, X., Liu, S., Peng, S., Xie, M.: The anti-jamming method based on front-back-edge tracking of vgpo jamming. In: 2016 CIE International Conference on Radar (RADAR), pp. 1–4 (2016)
19. Xingyu, Y., Huailin, R., Haoran, F.: A recognition algorithm of deception jamming based on image of time-frequency distribution. In: 2017 7th IEEE International Conference on Electronics Information and Emergency Communication (ICEIEC), pp. 275–278 (2017)
20. Abatzoglou, T.: Fast maximum likelihood joint estimation of frequency and frequency rate. In: ICASSP '86. IEEE International Conference on Acoustics, Speech, and Signal Processing, vol. 11, pp. 1409–1412 (1986)
21. Shie Qian, Dapang Chen, Qinye Yin: Adaptive chirplet based signal approximation. In: Proceedings of the 1998 IEEE International Conference on Acoustics, Speech and Signal Processing, ICASSP '98 (Cat. No.98CH36181), vol. 3, pp. 1781–17843 (1998)
22. Wang, P., Li, H., Djurovic, Himed: Performance of instantaneous frequency rate estimation using high-order phase function. IEEE Transactions on Signal Processing **58**(4), 2415–2421 (2010). doi:10.1109/TSP.2009.2034939
23. Xia, X.G.: Discrete chirp-fourier transform and its application to chirp rate estimation. IEEE Transactions on Signal Processing **48**(11), 3122–3133 (2000). doi:10.1109/78.875469
24. Guo, X., Sun, H.B., Wang, S.L., Liu, G.S.: Comments on discrete chirp-fourier transform and its application to chirp rate estimation [with reply]. Signal Processing IEEE Transactions **50**(12), 3115–3116 (2002). doi:10.1109/TSP.2002.805492
25. An, Y., Tian, B., Sun, Y.: An interference suppression algorithm based on a novel mdcft method for dsss system. In: 2008 9th International Conference on Signal Processing, pp. 1858–1862 (2008)
26. Berger, S.D.: Digital radio frequency memory linear range gate stealer spectrum. IEEE Transactions on Aerospace and Electronic Systems **39**, 1791–1801 (2003)
27. Bo, L., Yao, S., Chang-you, Z.: Study of multistatic radar against velocity-deception jamming. In: 2011 International Conference on Electronics, Communications and Control (ICECC), pp. 1044–1047 (2011)
28. Townsend, J.D., Saville, M.A., Hongy, S.M., Martin, R.K.: Simulator for velocity gate pull-off electronic countermeasure techniques. In: 2008 IEEE Radar Conference, pp. 1–6 (2008)
29. Pingyi Fan, Xiang-Gen Xia: A modified discrete chirp-fourier transform scheme. In: WCC 2000 - ICSP 2000. 2000 5th International Conference on Signal Processing Proceedings. 16th World Computer Congress 2000, vol. 1, pp. 57–601 (2000)

**Figures**

**Figure 1 The flowchart of recognition process to VGPO jamming signal.**

**Figure 2 The DCFT results of the target echo and VGPO jamming signal with various scaling factor $C$.** (a) Jamming (without scaling). (b) Target (without scaling). (c) Profiles of (a) and (b) after normalization. (d) Jamming ($C$=4e3). (e) Target ($C$=4e3). (f) Profiles of (a) and (b) after normalization. (g) Jamming ($C$=2e7). (h) Target ($C$=2e7). (i) Profiles of (g) and (h) after normalization.

**Figure 3 The estimated frequencies and chirp rates of target echo and jamming signal versus time.** (a) Linear scenario. (b) Non-linear scenario.

**Figure 4 The MSVR of target echo and VGPO jamming under different time width and pulse number.**

**Figure 5 Profiles of Fig. 4(b).**

**Figure 6 The MSVR of target echoes and VGPO jamming versus SNR.**

**Figure 7 The MSVR of the target echo and two kinds of jamming signals versus pulse number.**

**Figure 8 The identification probabilities of the proposed method under different pulse numbers and the method in [19].**

# Figures

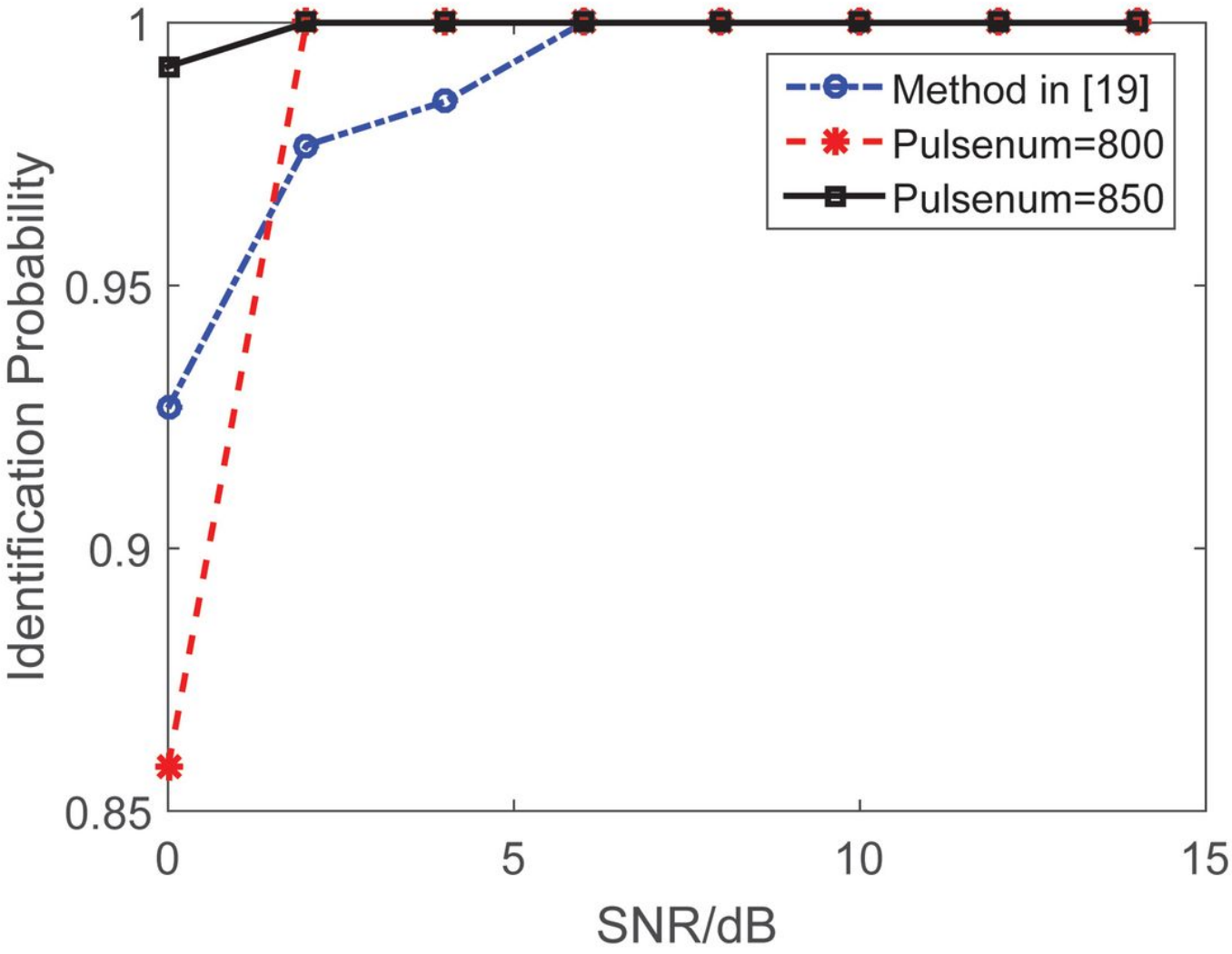


**Figure 1**

The identication probabilities of the proposed method under di erent pulse numbers and the method in [19].

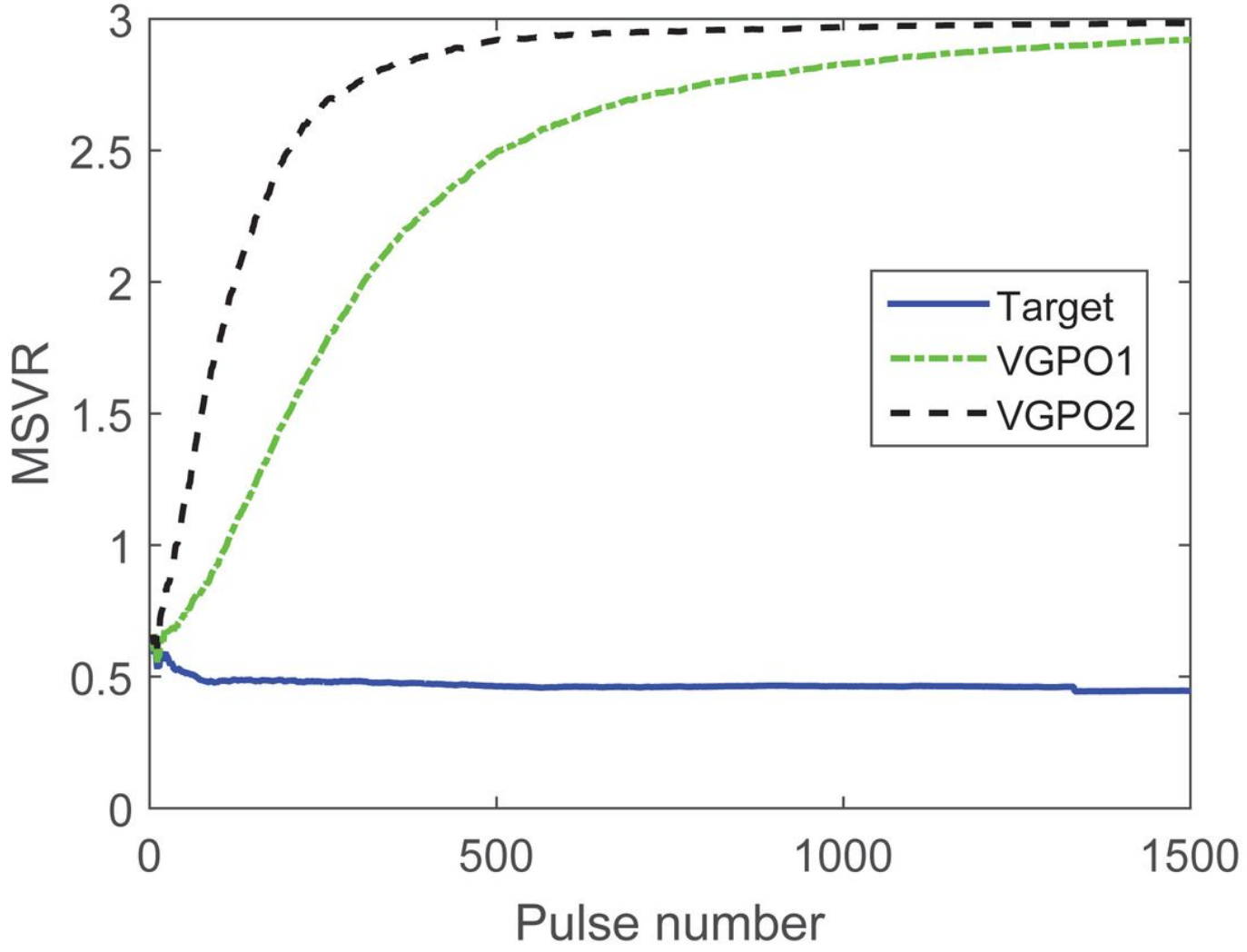


**Figure 2**

The MSVR of the target echo and two kinds of jamming signals versus pulse number.

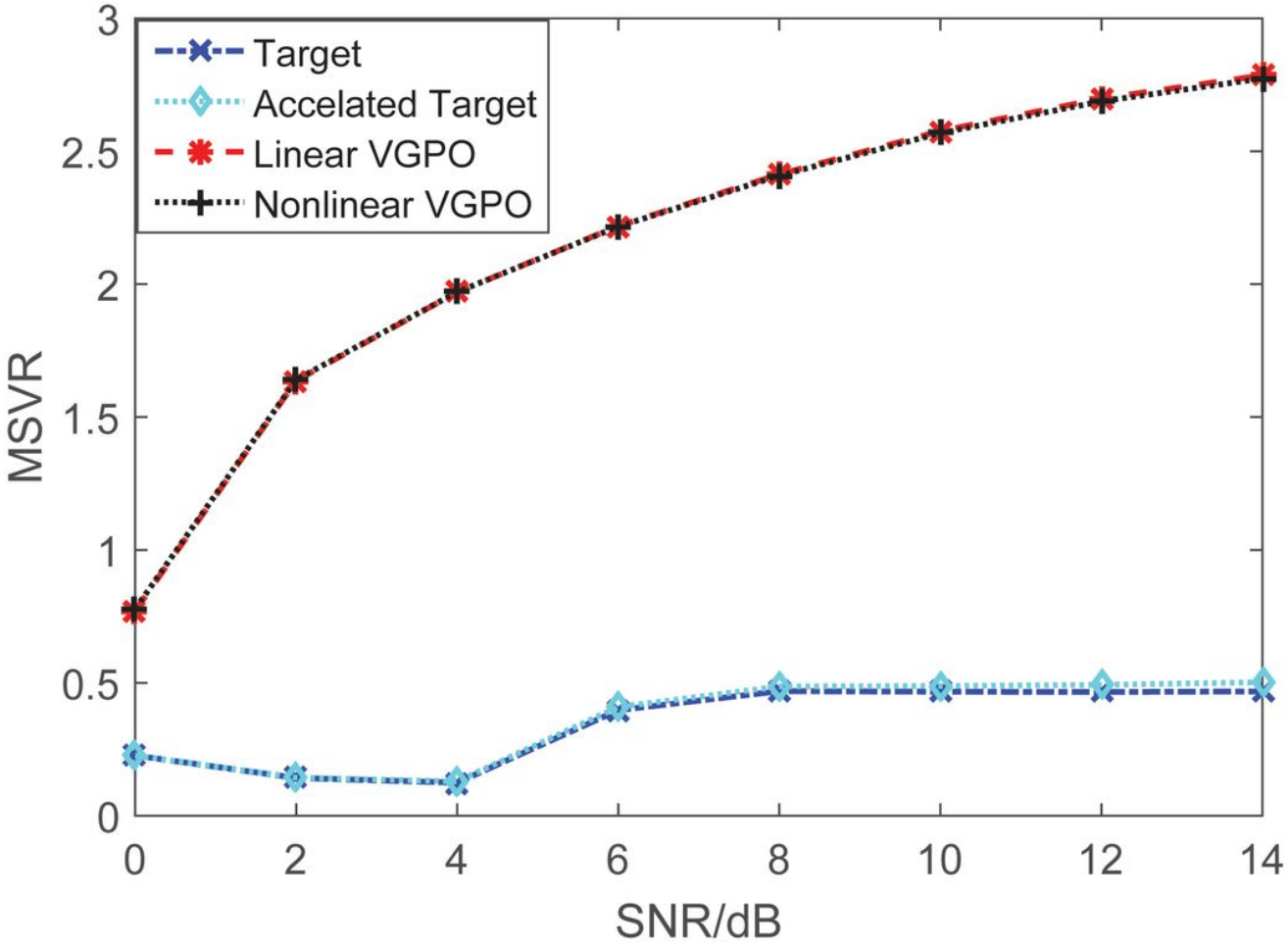


**Figure 3**

The MSVR of target echoes and VGPO jamming versus SNR.

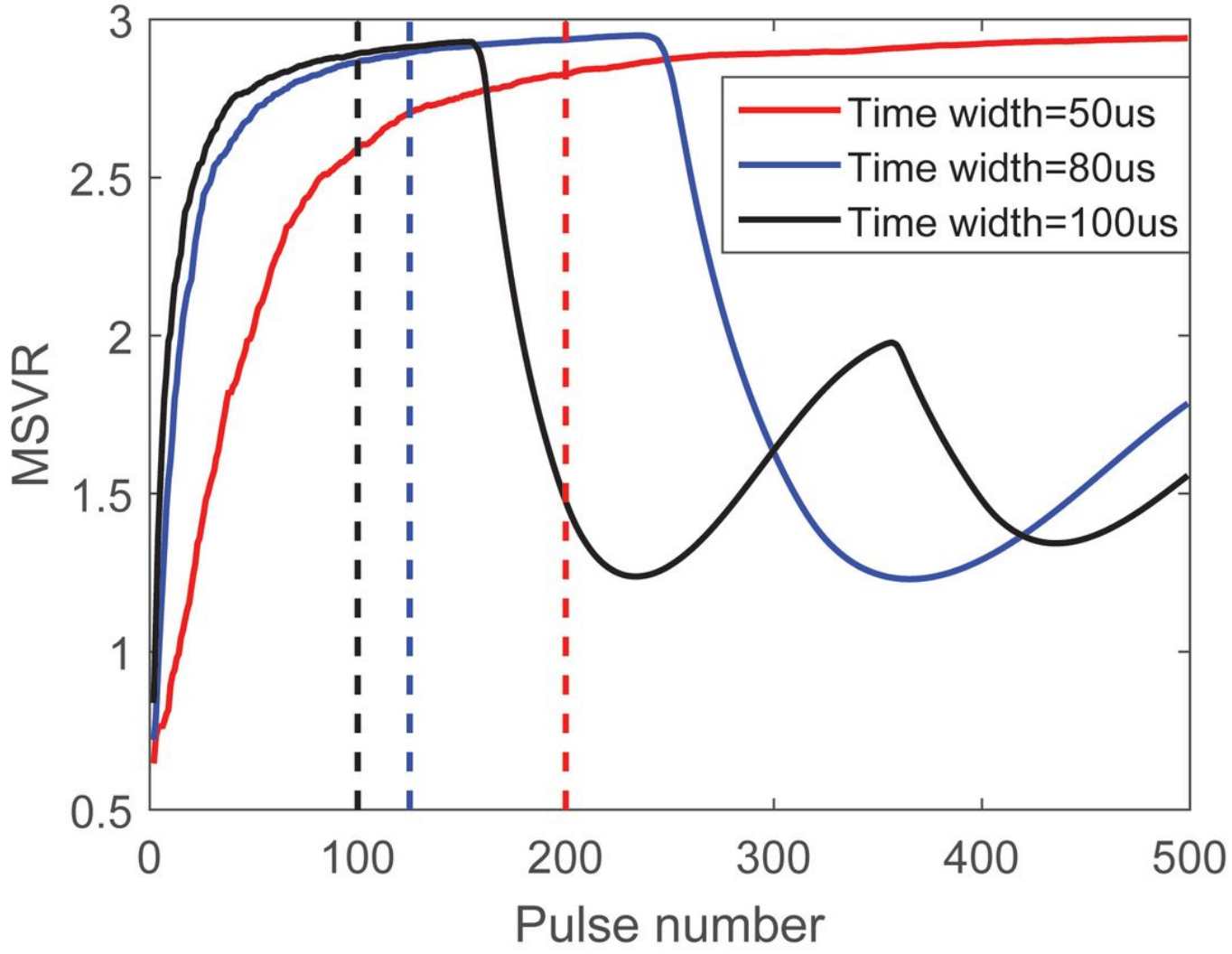


**Figure 4**

Profiles of Fig. 4(b).

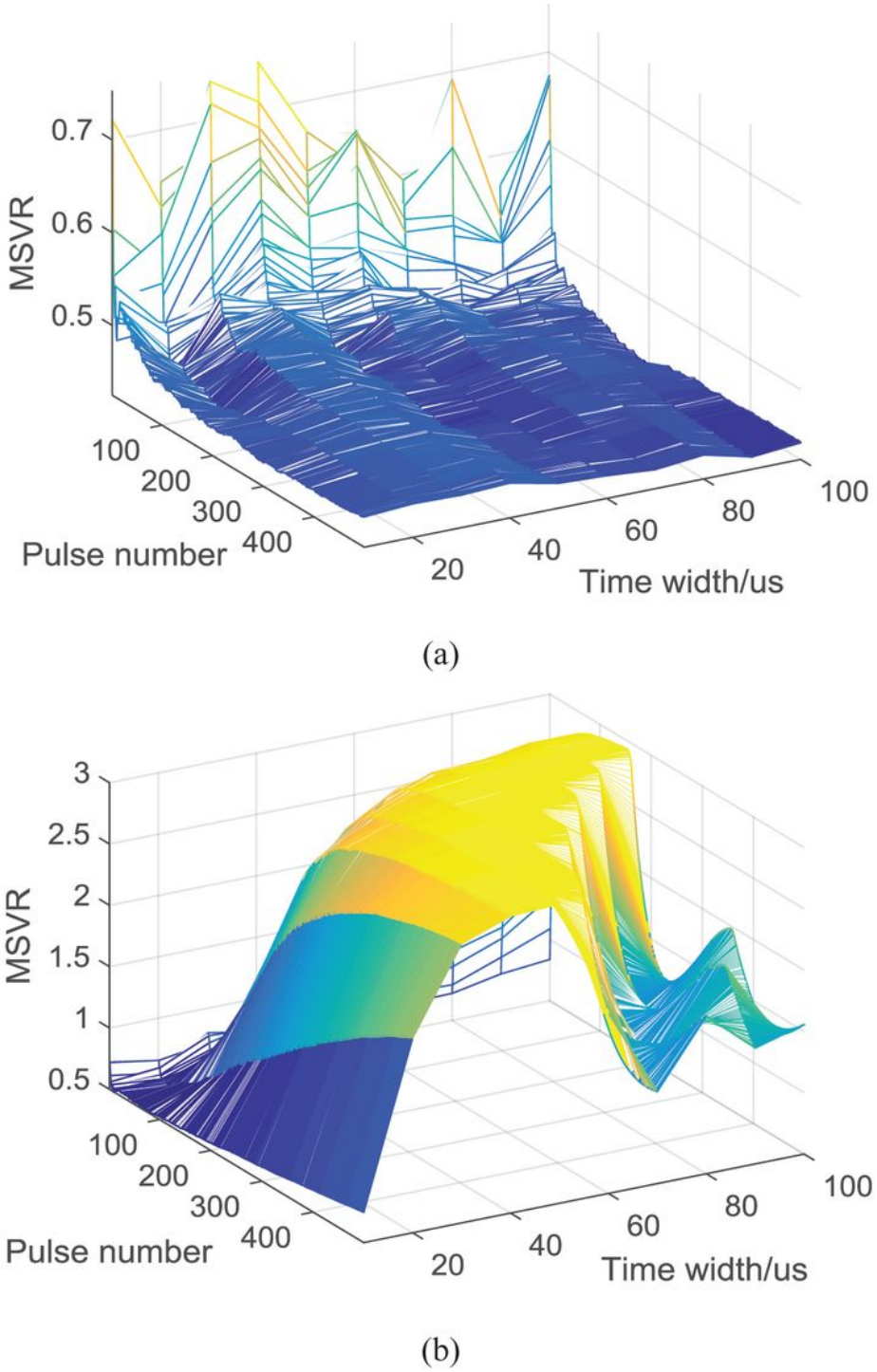


**Figure 5**

The MSVR of target echo and VGPO jamming under di□erent time width and pulse number.

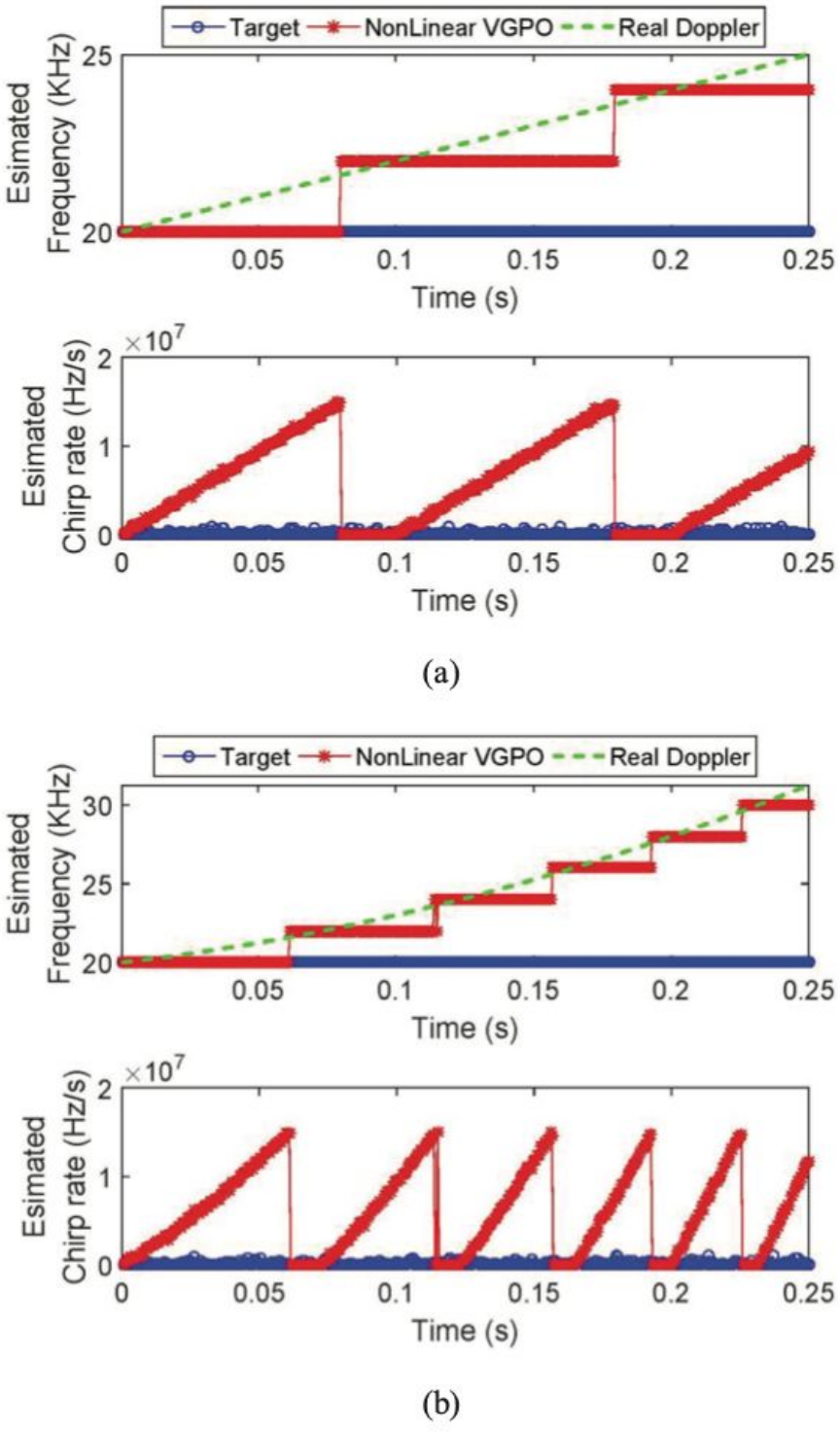


**Figure 6**

The estimated frequencies and chirp rates of target echo and jamming signal versus time. (a) Linear scenario. (b) Non-linear scenario.

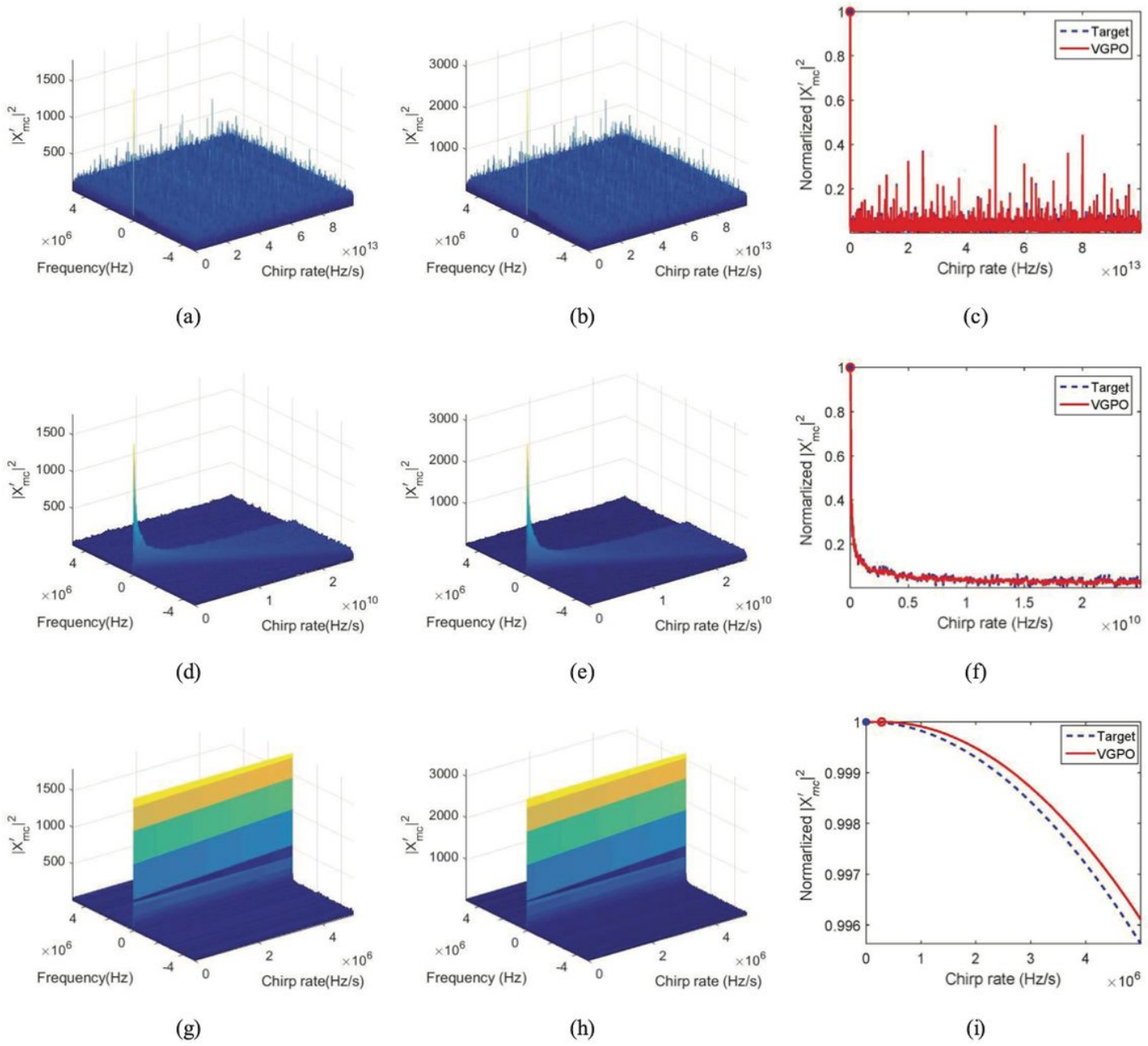


## Figure 7

The DCFT results of the target echo and VGPO jamming signal with various scaling factor. (a) Jamming (without scaling). (b) Target (without scaling). (c) Profiles of (a) and (b) after normalization. (d) Jamming (C=1e3). (e) Target (C=1e3). (f) Profiles of (a) and (b) after normalization. (g) Jamming (C=2e6). (h) Target (C=2e6). (i) Profiles of (g) and (h) after normalization.

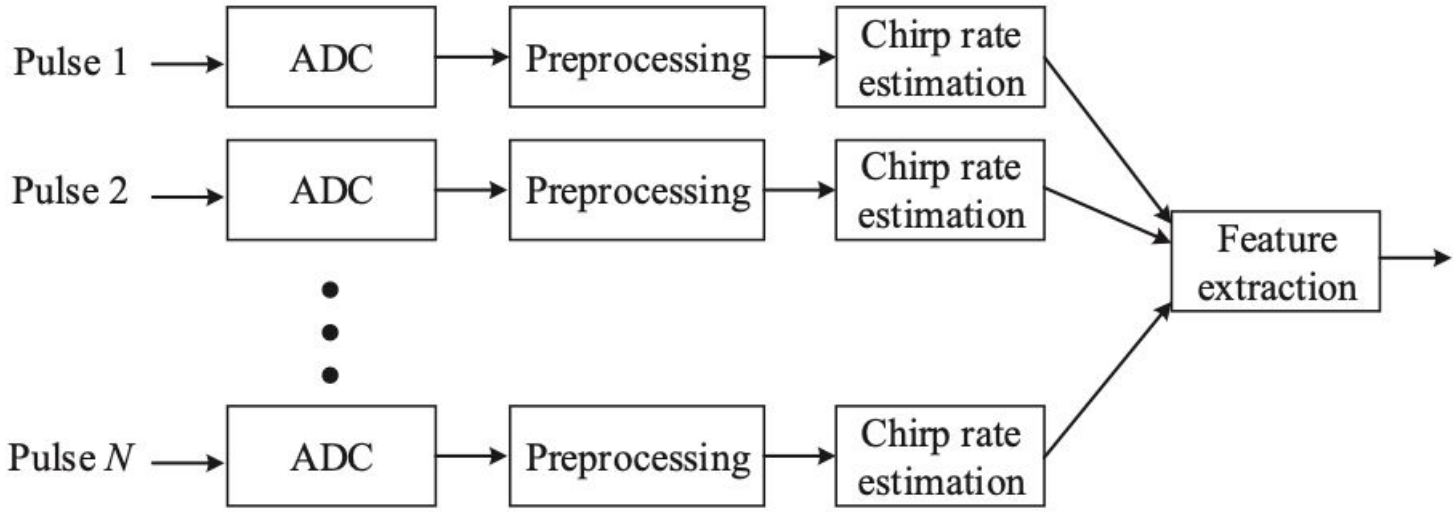


**Figure 8**

The flowchart of recognition process to VGPO jamming signal.

## Supplementary Files

This is a list of supplementary files associated with this preprint. Click to download.

- Supp.zip